Radiation Patterns of Unintentional Antennas: Estimates, Simulations, and Measurements*

Perry F. Wilson
Electromagnetics Division, National Institute of Standards and Technology
Boulder, CO 80305, USA
pfw@boulder.nist.gov

Abstract– **Electronic devices designed for purposes other than transmitting and receiving electromagnetic fields can act as unintentional antennas. Measurement methods are needed to characterize these antennas for electromagnetic compatibility tests; however, the rigor of precision antenna measurements is typically too costly and time consuming for electromagnetic compatibility applications. Alternate approaches are needed. This paper presents analytical estimates for the directivity of unintentional antennas based on the assumption that unintentional antennas will only randomly (and not coherently) excite the available propagating spherical modes at a given frequency. This directivity estimate is then compared to simulated and measured data. Good agreement is shown. Directivity estimates combined with simple total radiated power measurements represent a useful alternative to direct antenna measurements for electromagnetic compatibility tests.**

I. Introduction

Antennas are typically designed to have specific characteristics, such as gain or pattern, that are optimized for their intended use. However, electronics designed for other uses, such as digital devices, can also act as antennas. Thus, measurement methods are needed to determine the radiation patterns of unintentional antennas. Electromagnetic compatibility (EMC) standards have been developed to test and limit unintentional coupling to and from electronic devices (interference). However, present EMC emissions test methods are based largely on an interference scenario (broadcast television and radio below 1 GHz) which no longer represents the full interference environment.

Measurements on unintentional antennas present a number of challenges when compared to normal antenna tests. Information is needed throughout very large bandwidths (e.g., 30 MHz to 5 GHz). The direction of maximum radiation is not known by design. In principal, all pattern directions need to be checked, even though only the direction of maximum coupling is of interest. In practice, EMC emissions measurements on unintentional antennas need to be fast to make and inexpensive. Thus, traditional precision antenna measurements, such as spherical near-field scans, are not practical. Alternative approaches are needed.

This paper first discusses an estimate for the directivity of an unintentional antenna. The paper then presents simulations of an unintentional emitter and compares simulated directivity to the analytical estimate. The paper then presents measured data on a test object constructed to act as an unintentional emitter and again compares directivity results to analytical estimates. The implications of these data are then discussed.

II. Unintentional Antennas: Directivity Estimate

The expected maximum directivity of an unintentional emitter may be estimated by evaluating the far-field form of the spherical mode expansion of the emitter under the assumption that the expansion coefficients are independent random variables. We begin with the general form for the far-field pattern which may be found in various texts (e.g., Ch. 2 in [1])

$$\overline{E}(r,\theta,\vartheta) = k\sqrt{\eta}\,\frac{1}{\sqrt{4\pi}}\,\frac{e^{jkr}}{kr}\sum_{smn} Q_{smn}^{(3)}\,\overline{K}_{smn}(\theta,\vartheta), \quad (1)$$

where the spherical coordinate system is defined in the usual manner, η is the free space wave impedance, $\sum_{smn} = \sum_{s=1}^{2}\sum_{n=1}^{N}\sum_{m=-n}^{n}$, $N \approx ka$, where a is the radius of the minimum sphere enclosing the emitter (it is assumed the spherical coordinate system is centered in this sphere), $Q_{smn}^{(3)}$ are the wave coefficients, and $\overline{K}_{smn}(\theta,\vartheta)$ are the far-field, large argument, forms of the dimensionless power-normalized spherical wave functions [1]. This convention yields the simple expression

$$P_{rad} = \frac{1}{2}\sum_{smn}\left|Q_{smn}^{(3)}\right|^2 \quad (2)$$

for the total radiated power P_{rad} from the emitter. In general the summation over n goes to infinity; however, spherical wave functions with indices $n > ka$ are cut off and will not contribute in the far-field and, thus the series can be truncated.

The total number of modes N_m for the truncated series is

$$N_m = 2\sum_{n=1}^{N}(2n+1) = 2(N^2+2N). \quad (3)$$

The number of samples N_s to determine the wave coefficients is twice N_m, since each coefficient has an independent real and imaginary part.

These expressions can first be used to find an upper bound for directivity, as derived in [1] (eq. 2.225). Directivity is expressed as the ratio of the radiated power at a given angle and distance (using eq. (1)) to the total radiated power (using eq. (2)) divided by the total solid angle (4π steradians). An application of the Cauchy-Schwartz inequality yields a sum over the number of modes (3) that is reduced by a factor of two due to polarization mismatch to the spherical modes. This yields the result below once (ka) is substituted for N:

$$D_{max} \approx \begin{cases} 3, & ka \le 1 \\ (ka)^2 + 2ka, & ka > 1 \end{cases} . \qquad (4)$$

While D_{max} is a good upper bound for intentional emitters, such as high gain antennas, it will significantly overestimate directivity for the unintentional emitters of interest in EMC measurements. A better estimate for EMC purposes can be derived as follows by assuming that the spherical-wave coefficients are independent random variables.

Directivity D is the sum of the co- and cross-polarized terms [1-2]

$$D = D_{co} + D_{cross} . \qquad (5)$$

For unintentional emitters the mean values of the co- and cross-polarized terms will be equal, and because the mean value of D is 1, we have

$$\langle D_{co} \rangle = \langle D_{cross} \rangle = \frac{1}{2} . \qquad (6)$$

Returning to (1), the field components can be written

$$\begin{aligned} \left|\overline{E}_\theta(r,\theta,\vartheta)\right|^2 &= \frac{\eta}{4\pi r^2}\left|\sum_{smn} Q^{(3)}_{smn}\,\overline{K}_{smn}(\theta,\vartheta)\cdot\overline{a}_\theta\right|^2 \\ \left|\overline{E}_\vartheta(r,\theta,\vartheta)\right|^2 &= \frac{\eta}{4\pi r^2}\left|\sum_{smn} Q^{(3)}_{smn}\,\overline{K}_{smn}(\theta,\vartheta)\cdot\overline{a}_\vartheta\right|^2 \end{aligned} . \qquad (7)$$

For an unintentional emitter we will assume that that the real and imaginary parts of $Q^{(3)}_{smn}$ are independent and Gaussian distributed with zero mean. Under this assumption the field components will be chi squared distributed with two degrees of freedom. The directivities D_{co} and D_{cross} will be similarly distributed. It is shown ([3], Appendix B) that the expected value for the maximum over N_s samples of a chi square with two degrees of freedom distribution (using D_{co} as an example) is:

$$\langle D_{co,\max} \rangle = \langle D_{co} \rangle \sum_{n=1}^{N_s} \frac{1}{n} . \qquad (8)$$

This summation can be approximated (e,g., [4] eq. 0.131) and substituting the expected value of D_{co} from (6) yields

$$\langle D_{co,\max} \rangle \approx \frac{1}{2}\left[0.577 + \ln(N_s) + \frac{1}{2N_s}\right] . \qquad (9)$$

This is the result for $ka > 1$, noting that $N_s = 2N_m$ and setting $N = ka$ in (3). For $ka = 1$ ($N_s = 12$), (9) yields $\langle D_{co,\max} \rangle \approx 1.55$. A physical interpretation of $N_s = 12$ for $ka \le 1$ is that the real and imaginary parts of six dipole moments (three electric and three magnetic) yield 12 independent source contributions. The directivity estimate is also very near the directivity of a single short dipole (D = 1.5). Thus, using 1.55 for electrically small emitters in (9) results in a continuous function and should give good estimates for directivity:

$$\langle D_{\max} \rangle \approx \begin{cases} 1.55, & ka \le 1 \\ \dfrac{1}{2}\left[0.577 + \ln\left(4(ka)^2 + 8ka\right) + \dfrac{1}{8(ka)^2 + 16ka}\right], & ka > 1 \end{cases} . \qquad (10)$$

The key difference between the intentional emitter upper bound given by (4) and the unintentional emitter expected value given by (10) is that the upper bound increases rapidly as the square of the electrical size ka, while the expected value increases only as the natural logarithm (ln) of electrical size ka.

A result for a planar cut is found in a similar manner. If we orient the coordinates so that the (r,φ) plane coincides with the cut, then we need only account for the $2N+1$ φ-dependent modes. The number of complex coefficients to be determined is again twice this number, $N_c = 2(2N+1)$. The received power will again be chi squared distributed with two degrees of freedom. Thus, (8) yields

$$\frac{\langle P_{rec,\max} \rangle}{\langle P_{rec} \rangle} \approx \begin{cases} 2.45, & ka \le 1 \\ 0.577 + \ln\left(4(ka) + 2\right) + \dfrac{1}{8(ka) + 4} & ka > 1 \end{cases} \qquad (11)$$

for ka > 1. Taking the limit at $ka = 1$ ($N_c = 6$) as the approximation for electrically small emitters yields the lower limit in (11). This result is particularly useful, as planar cut measurements are more readily made than full three dimensional scans.

III. Unintentional Antennas: Simulated Directivity

A simple model of an unintentional emitter can be used to generate directivity data for comparison to the above theoretical estimates. We will here simulate an unintentional emitter as a set of isotropic point sources randomly distributed on the surface of a sphere (coordinates θ,φ) of radius a. Each

source has random magnitude I and phase α. All variables are uniformly distributed over their respective ranges:

$$\theta \in [0,\pi], \quad \varphi \in [0,2\pi], \quad I \in [0,1], \quad \alpha \in [0,2\pi]. \quad (12)$$

The far-field received power from this source set [5] is proportional to

$$P_{rec}(\theta,\varphi) = \left| \sum_{i=1}^{N} I_i e^{j(ka\cos\psi_i + \alpha_i)} \right|^2, \quad (13)$$

where $\cos\psi_i = \cos\theta\cos\theta_i + \sin\theta\sin\theta_i\cos(\varphi - \varphi_i)$ and (θ_i,φ_i) identifies the location of the ith source. This model loosely simulates an enclosure with various electrically small surface sources, due to apertures, seams, connectors, etc.

As an example, consider the following case. Assume a test object diameter of 50 cm (a = 25 cm), a set of five sources, and an upper frequency limit of 5 GHz ($ka \approx 26$). The above expression can be used to simulate the results from a planar cut (1˚ angular steps) for comparison to the estimate given by equation (11). The results for a single simulation run are shown in Figs. 1-3. Fig. 1 shows the radiation pattern at the upper-frequency end (ka = 26) over a representative planar cut. Note that the pattern shows multiple narrow lobes. Fig. 2 shows the theoretical (11) and simulated ratios of the maximum-to-mean received power over the planar cut chosen. The simulated data have some values above the theoretical estimate, demonstrating the statistical variation about the expected value for maximum directivity.

We used the above parameters (five sources, a = 0.25 cm, $ka \approx 26$) in a Monte Carlo simulation of 100 runs to determine an average value for $P_{rec,max}/\langle P_{rec}\rangle$ that can be compared to the theoretical estimate (11). The results are given in Fig. 3, which shows that the theory gives a conservative upper bound on the mean value for the case of five sources. If we increase the number of sources to 50, then simulated maximum-to-mean received power more closely approaches the theoretical estimate, as shown in Fig. 4.

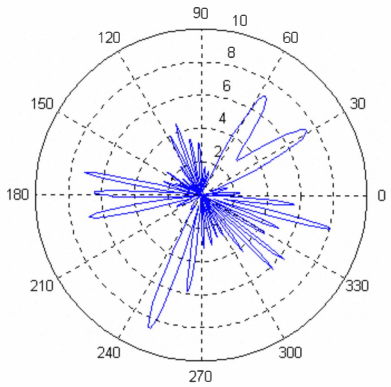

Fig. 1 The radiation pattern (x-z axes plane) for a set of five arbitrary sources located on a sphere of radius 0.25 m at 5 GHz ($ka \approx 26$).

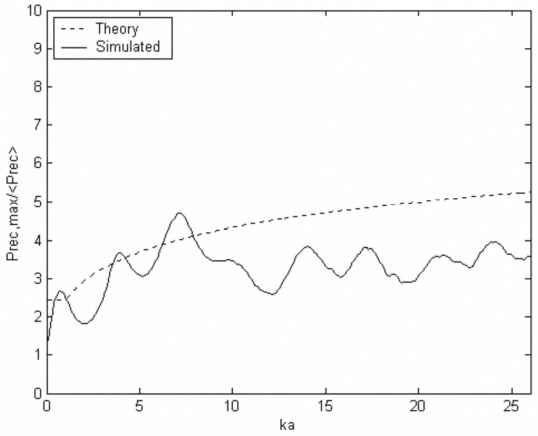

Fig. 2 The estimated (theory) and simulated $P_{rec,max}/\langle P_{rec}\rangle$ ratios for the same set of sources as used in Fig. 1.

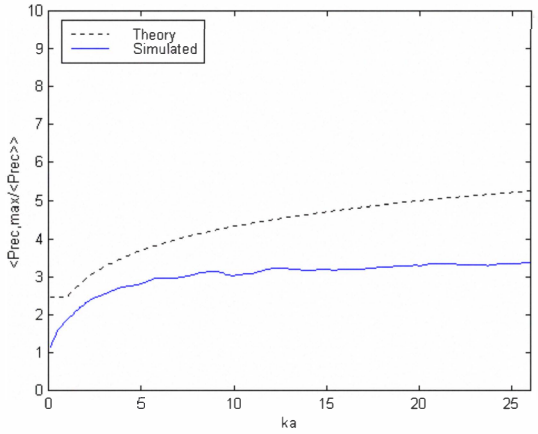

Fig. 3 The estimated and simulated $\langle P_{rec,max}/\langle P_{rec}\rangle\rangle$ ratio for five arbitrary isotropic sources randomly placed on a sphere of radius 0.25 m, from a Monte Carlo run of 100 simulations.

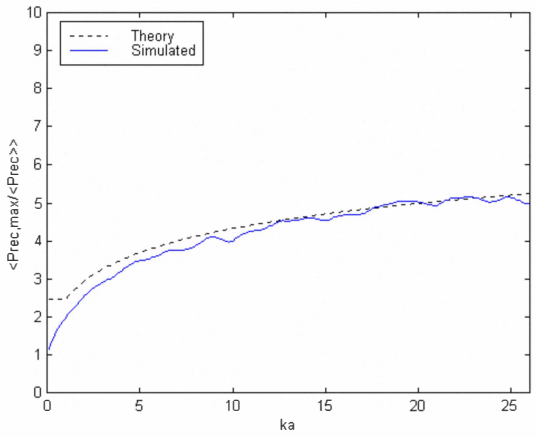

Fig. 4 The estimated and simulated $\langle P_{rec,max}/\langle P_{rec}\rangle\rangle$ ratio for 50 arbitrary isotropic sources randomly placed on a sphere of radius 0.25 m, from a Monte Carlo run of 100 simulations.

IV. Unintentional Antennas: Measured Pattern Data

To further investigate pattern and directivity for unintentional emitters, a simple test object was constructed and its antenna pattern was measured over various planar cuts. The test object consisted of a rectangular metallic box (0.73 x 0.93 x 1.03 m) with five holes of 1.5 cm diameter randomly placed on each face, making a total of 30 holes. A horn antenna, driven by a signal generator connected via a coaxial cable to a connector on a face of the box, excited the box interior. Numerous planar cuts were measured from 2 GHz to 4 GHz in 40 MHz steps.

Fig 5 shows representative planar cuts for the 30-hole EUT at 2 GHz. The patterns show multiple lobes with no favored pattern direction. This pattern is very representative of EMC test objects. Such patterns send a bad news, good news message to EMC test engineer. The bad news is that the patterns are complex and vary rapidly with frequency. Full three dimensional scans are needed at each frequency to determine the true absolute maximum. The good news is that the many lobes tend to be similar in strength. Thus, finding several representative lobes may give a good estimate of the overall strongest lobe. Stated alternatively, an unintentional emitter is expected not to exhibit strong directivity, as it is not designed to do so.

The 30-hole test object has an internal paddle to change the distribution of the aperture excitation. This allows us to generate statistics, as if different EUTs were being measured. Fig. 6 shows the average results similar to Figs. 3 through 4 for the maximum-to-mean received power based on 48 random pattern measurements. The measured data closely approach the theoretical estimate, much as shown in Fig. 4, where the source number was also high. We can also simulate the 30-hole test object using 15 random sources (we assume that the metallic case mostly shields the backside apertures) and a sphere radius of 0.784 m (based on the EUT diagonal). Fig. 6 also shows the result for a Monte Carlo simulation of 48 tests based on these parameters. The simulation well mimics the characteristics of the measured data.

V. Conclusion

The good agreement between theory, simulation, and measurement validates the statistical approach used here. Therefore, equations (10) through (11) can be used to reasonably estimate the maximum directivity of an unintentional emitter based on its electrical size (*ka*). If the total radiated power from a test object has been measured, for example in a reverberation chamber, then simple expressions can be used to estimate the maximum electric field at a given distance for EMC applications, namely,

$$\left\langle E_{\max}^2 \right\rangle = \left\langle D_{\max} \right\rangle \frac{\eta}{4\pi r^2} P_{rad} \ , \qquad (14)$$

where $D_{\max}$ is given by (10). This approach could form a good basis for future EMC standards at higher frequencies, where EUT pattern complexity makes present approaches either too time-consuming (too many measurement points) or inaccurate (maximum field not determined).

Acknowledgement

This paper is largely derived from an earlier publication [3] co-authored by myself, David Hill, and Chris Holloway of NIST. Their significant contributions to this work are gratefully acknowledged.

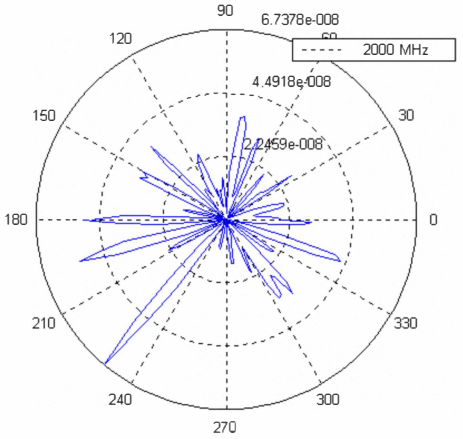

Fig. 5 Measured radiation pattern for the 30-hole box at 2 GHz.

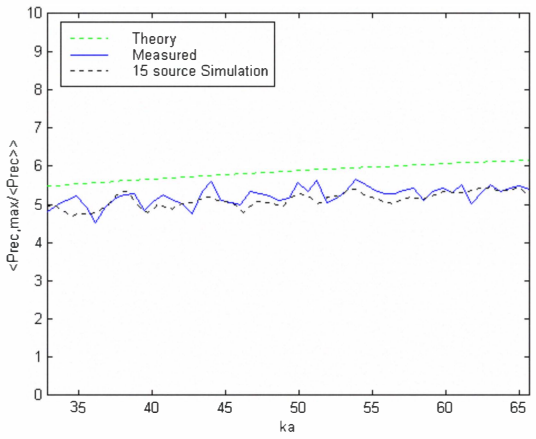

Fig. 6 The estimated (theory), measured, and simulated (15 sources) $P_{rec,max}/\langle P_{rec}\rangle$ ratio for the 30-hole EUT.

References

[1] J. Hansen, Ed., Spherical Near-Field Antenna Measurements, Peter Peregrinus: London, UK, 1988.

[2] G. Koepke, D. Hill, and J. Ladbury, "Directivity of the test device in EMC measurements," Proc. 2000 IEEE Intl. Symp. on EMC (Wash., DC), pp. 535-539, Aug. 2000.

[3] P. Wilson, D. Hill, and C. Holloway, "On determining the maximum emissions from electrically large sources," IEEE Trans. on EMC, vol. 44, no. 1, pp. 79-86, Feb. 2002.

[4] I. Gradshteyn and I. Ryzhik, Table of Integrals, Series, and Products, Academic Press, San Diego, CA, 1980.
[5] M. Ma, Theory and Application of Antenna Arrays, Wiley & Sons, New York, 1974.